Rare Metal Materials and Engineering
Volume 48, Issue 4, April 2019
Available online at www.rmme.ac.cn

Science Press

Cite this article as: Rare Metal Materials and Engineering, 2019, 48(4): 1116-1123.

ARTICLE

Influence of Fiber Size and Interface Morphology on the Electrochemical Corrosion Resistance of Directionally Solidified NiAl-9Mo Eutectic Alloy

Guo Junbo, Zhong Hong, Liu Zhenpeng, Yang Luyan, Li Shuangming

State Key Laboratory of Solidification Processing, Northwestern Polytechnical University, Xi'an 710072, China

Abstract: As the solidified microstructures have a significant influence on the corrosion behavior, the present work is thereby aimed to derive the optimum microstructures and electrochemical conditions for producing Mo nanowires. Eutectic microstructures showing coupling growth of NiAl phase and Mo fibers were obtained at growth rates from 10 μm/s to 40 μm/s. The fiber size varies from 800 nm to 300 nm, and decreases with the increase of solidification rate. The results of potentiodynamic polarization studies indicate that NiAl-Mo alloy at a growth rate of 20 μm/s has a better corrosion resistance in 0.1 mol/L HCl solution at room temperature. The electrochemical corrosion behavior of directionally solidified NiAl-Mo alloys not only depends on fiber size, but also relates to the interface morphology. To further analyze the influence of interface morphology on the corrosion behavior, velocity sudden change experiments were carried out. The microstructure of directionally solidified NiAl-Mo alloy transforms from planar to cellular and dendritic structures as the value of V/V_1 increases. The results of potentiodynamic polarization curves reveal that the planar structure has the highest corrosion resistance compared to other morphologies with the same fiber size of Mo-nanowires.

Key words: directional solidification; NiAl-Mo eutectic alloy; interface morphology; corrosion resistance

Nanostructured materials have captured the attention of researchers because of their unusual properties when the feature size falls below a certain value. One-dimensional metallic nanowires show this favorable behavior on promising mechanical, electronic and optical performance in the range of a few hundred nanometers[1]. The intrinsic properties of nanowires can be tuned by controlling size, shape, periodic arrangement and crystallinity[2]. There are many reports about fabrication of the nanostructured materials through different routes, such as chemical and electrochemical deposition[3-5]. However, these methods cannot well adjust nanowire size. These nanowires are usually polycrystalline, which often restricts their applications. For example, spectroscopic properties of nanowires cannot come true because of the different adsorption abilities for molecules on different crystallographic surfaces[6].

Recently, a method was established to fabricate single crystalline and self-organized nanowires with a high aspect ratio from directionally solidified eutectic alloy[7-9]. Hassel et al[7] produced W-nanowire arrays through a directionally solidified eutectic NiAl-W alloy, followed by a phase separation by selective dissolution of the NiAl matrix to release tungsten nanowires from the matrix with a wire diameter of about 200 nm. The aspect ratio (length/diameter) was more than 400. Further, wire diameter and spacing can be controlled by adjusting the solidification parameters. Milenkovic et al[10] studied the effect of growth conditions on the spatial features of Re nanowires produced by directional solidification and found that both the spacing and diameter increase with decreasing growth rate and temperature gradient. Note that the growth rates have an important influence on the eutectic microstructure. Nanostructured eutectic corrosion behavior largely depends upon the microstructure. Osório et al[11] have demonstrated that microstructural features play an

Received date: April 20, 2018
Foundation item: National Natural Science Foundation of China (51674201)
Corresponding author: Zhong Hong, Ph. D., Professor, State Key Laboratory of Solidification Processing, Northwestern Polytechnical University, Xi'an 710072, P. R. China, Tel: 0086-29-88493264, E-mail: zhonghong123@nwpu.edu.cn

important role in the general corrosion resistance of Al-Ni alloys. Peixoto et al[12] found that coarse cells associated with lower cooling rates have better corrosion resistance than fine cells which are related to higher cooling rates for Pb-Sn alloys. Understanding the role of different solidification velocities is imperative to control the final microstructure of eutectic alloys. The evolution of a solidification microstructure in a metallic system can be characterized by different growth morphologies, such as planar, cellular and dendritic growth. Gail et al[13] found that a transition from a planar solid-liquid interface to cellular solidification occurred between 50 and 60 mm/h at the rotation speed of 60 r/min for directionally solidified NiAl-Mo eutectic alloy. In order to derive the optimum conditions for producing nanowires, it is important to find out the relationship between corrosion behavior and solidified microstructure developed with growth rates.

Directionally solidified NiAl-Mo alloy, comprising an array of self-organized Mo fibers in the NiAl matrix, is a promising way to fabricate Mo nanowires. In the present work, the results of experimental studies in NiAl-Mo eutectic alloy were investigated with a focus on the following major points: (a) the variation of fiber spacing range with growth velocity, to farther clarify fiber diameter selection criterion; (b) the corrosion behavior of the NiAl-Mo eutectic alloy with different fiber size; (c) changing interface morphologies with constant fiber size through abrupt changing of solidification rate in directional solidification experiments, thus clarifying the influence of morphology on corrosion behavior and obtaining corrosion mechanisms of NiAl-Mo alloy.

1 Experiment

Pre-alloys were prepared from nickel (99.96%), electrolytic aluminum (99.99%) and molybdenum (99.96%) by induction melting under an inert atmosphere. The ingot was about 80 mm in diameter and 100 mm in length. The directional solidification samples were cut from the master ingot into *Φ*7 mm×100 mm cylinder bars by a wire electro-discharged machine, which was performed in an improved Bridgman vertical vacuum furnace described in Ref. [14]. In the process of directional solidification, the samples were heated by a graphite heater at 1900±10 K and a thermal gradient of approximately 300 K/cm. Some samples were directionally solidified at growth rates of 10, 20 30 and 40 μm/s. The others were solidified firstly at a growth rate of 2 and 5 μm/s. After the solidified distance reached 30 mm, the growth rate was suddenly changed to 20 μm/s to stabilize the growth state, and then the samples were quenched rapidly by pulling into a liquid Ga-In-Sn pool.

The directionally solidified samples were cut transversely and longitudinally, and representative samples were mounted in epoxy. The metallographic process involved grinding, mechanical polishing and chemical etching with a solution of 80%HCl-20%HNO_3 by volume. The etched specimens were examined by both optical microscopy and scanning electron microscopy (SEM). The microstructures were analyzed using image analysis software to measure the fiber size.

The electrochemical polarization was performed in an electrochemical workstation (PGSTAT 4000) of a three-electrode cell using the sample as the working electrode (0.2 cm^2), platinum sheet as the counter electrode and Ag/AgCl in saturated potassium chloride (KCl) as the reference electrode in 0.1 mol/L HCl solution. The Ag/AgCl-reference electrode is 0.197 V lower than the standard hydrogen electrode (SHE)[15].

Potentiodynamic polarization measurements were made from an initial potential of –0.5 V versus the open current potential (OCP) to a final potential of 2 V versus the reference potential. Unless notified in the paper, all potential recorded were referred to a silver/silver chloride (Ag/AgCl) electrode in saturated KCl (0.197 V SHE). And a scanning rate was obtained as 1 mV/s during all measurements.

After the polarization experiment, the samples were cleaned by distilled water and then dried. Then the etched specimens were investigated by scanning electron microscopy.

2 Results and Discussion

2.1 Microstructure of directionally solidified NiAl-Mo

In the present study, the NiAl-Mo alloy exhibits a fibrous microstructure, being similar to what has been reported in Ref. [13,16,17]. Fig.1 shows the steady-state microstructures in the transverse sections obtained at different growth rates (10, 20, 30 and 40 μm/s). The arrangement of the Mo fiber in cross-section is approximately hexagonal. The shape of the individual Mo fiber is not circular but square, which indicates the NiAl-Mo interfacial energy is highly anisotropic. And it can be seen that the typical quenched solid-liquid interfaces remain planar only for growth rates up to 20 μm/s. At the higher growth rate of 30 μm/s, the solid-liquid interfaces are cellular. It suggests that a transition to cellular solidification occurs between 20 and 30 μm/s. According to the theory of constitutional supercooling:

$$\frac{G_L}{V} \geq -\frac{m_L(C_E - C_0)}{D} \quad (1)$$

where, G_L is the temperature gradient in the liquid ahead of the interface, D is the inter-diffusion coefficient, V is the growth rate, m_L is the slope of the liquidus, C_E is the eutectic composition, and C_0 is the initial composition of the solidifying alloy. All the parameters on the right hand side of Eq.(1) are material constants. Therefore, for a given temperature gradient, the S/L interface can present instabilities for a larger growth rate.

In order to obtain more solid-liquid interfaces at a constant growth rate, dynamical experiments were carried out. Fig.2 shows macrographs in the longitudinal sections where the growth rate is then abruptly changed to V (V>V_1), and V is the final velocity of 20 μm/s. This solidification with a starting

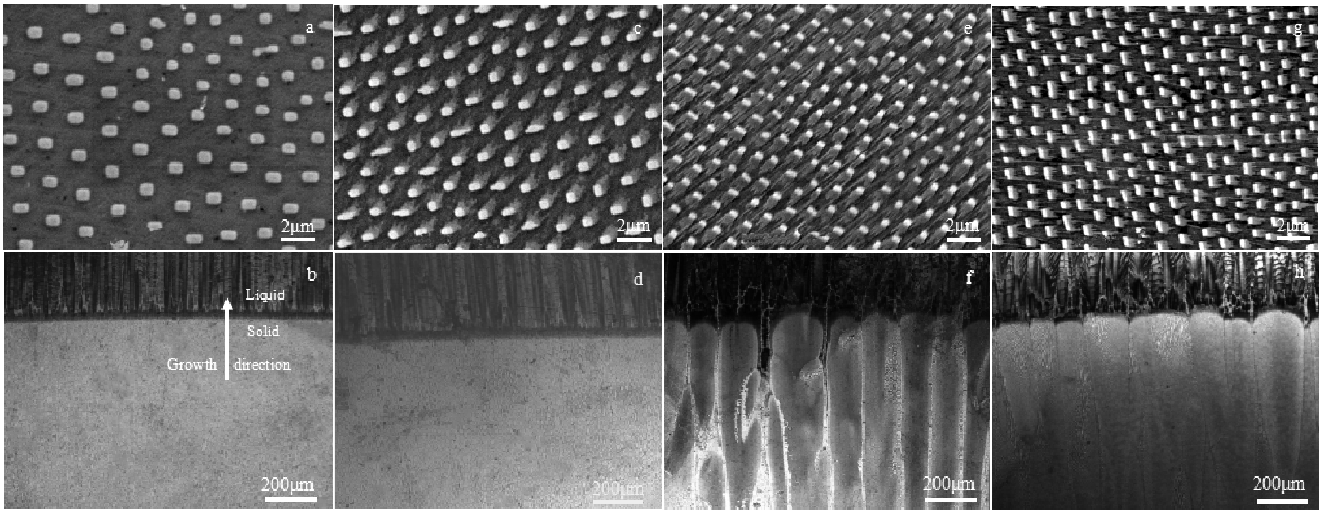

Fig.1 SEM micrographs in transverse section and quenched S/L interfaces of directionally solidified NiAl-Mo eutectic alloy at different growth rates: (a, b) V=10 μm/s, (c, d) V=20 μm/s, (e, f) V=30 μm/s, and (g, h) V=40 μm/s (dark phase-NiAl, light phase-Mo)

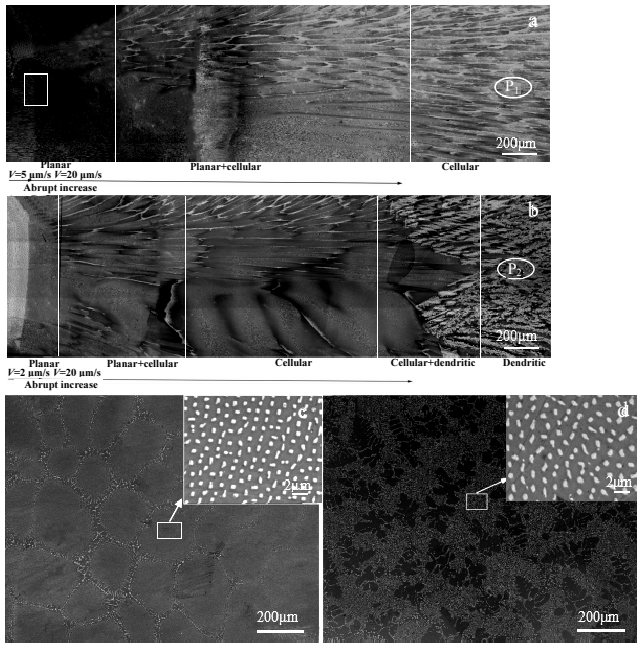

Fig.2 Typical macrostructures of directionally solidified NiAl-Mo alloys with two different values of V/V_1: (a) 5~20 μm/s and (b) 2~20 μm/s; transverse micrographs of the position P_1 in Fig.2a (c) and position P_2 in Fig.2b (d)

directional solidification rate of 5 μm/s (V/V_1=4) produces a microstructure with three distinct zones (planar, planar+ cellular and cellular zones) as shown in Fig.2a. When the initial velocity is 2 μm/s (V/V_1=10), the typical dendritic morphology with side-branches can be observed as shown in Fig.2b. Interestingly, the well-aligned microstructure, devoid of any cellular or dendritic regions, can be observed at the constant growth rate of 20 μm/s (Fig.1b).

Since the amount of solute carried ahead of the interface in the steady state case is more when the growth rate suddenly increases, there will be a transient rise in the concentration in the liquid near the interface. So when the solid is formed, the original steady state is destroyed and a new steady state is reconstructed.

Smith et al[18] has reported when the growth rate suddenly increased, the solute concentration in the liquid would increase and then decrease to a steady value in the front of the solid/liquid interface. Based on the theory of constitutional supercooling, Eq. (1) can be rewritten as:

$$C_{\mathrm{L}}^{\max} < -\frac{DG_L}{m_{\mathrm{L}}V(1-K)} \quad (2)$$

where, $C_{\mathrm{L}}^{\max}$ is the maximal solute concentration in the front of the solid/liquid interface, and K is the distribution coefficient. Therefore, the left hand side of Eq. (2) predicts that, for a given growth rate, the more the solute concentration gradient in the liquid ahead of the interface is, the less stable the interface is. Smith et al[18] indicated $C_{\mathrm{L}}^{\max}$ would increase with the value of V/V_1 increasing. This may explain why dendritic structure was obtained when the initial growth rate was 2 μm/s (2~20 μm/s), whereas only cellular microstructure was obtained when the initial velocity was 5 μm/s (5~20 μm/s).

Fig.3 shows the interface morphology of directionally solidified NiAl-Mo eutectic alloy where the growth rate changes from 5 μm/s to 20 μm/s. With the rate of growth suddenly increases, the fiber size decreases clearly at once. The eutectic spacing was adjusted to achieve another steady state through some mechanism. The mechanism includes two parts: ending (arrow 1) and branching (arrow 2), even multiple

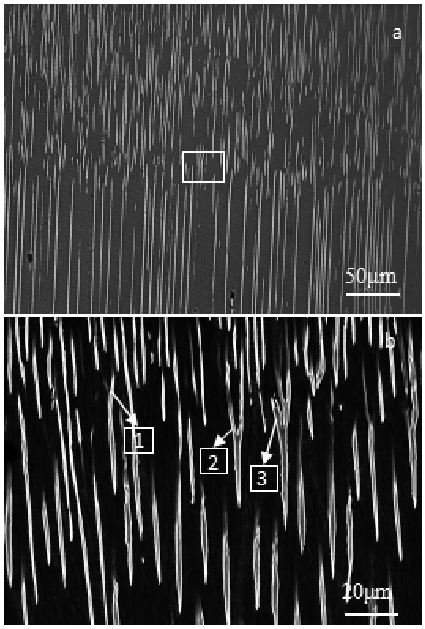

Fig.3 Interface morphologies of directionally solidified NiAl-Mo eutetic alloy when the growth rate was suddenly changed at a value of 5~20 μm/s: (a) interface overview and (b) close-up of the white square

branching (arrow 3) in local area, which improved greatly the adjustment process of fiber size. It doesn't present difficulties in the branching phenomenon for NiAl-Mo eutectic, which proves the problem of fiber size selection can be ignored, despite the presence of an intermetallic phase. Also, in the branches of the fibers, terminations are found in fibrous eutectics to obtain a constant inter-fiber spacing under steady-state growth conditions. The chemical potential of terminations is higher than that of branches due to their greater total curvature[19]. Therefore, material transport occurs from the terminations to branches with smaller curvatures. As a result, the interface is clear when the growth rate is abruptly changed and presents a retardative response of fiber diameter (α) to V.

Jackson and Hunt[20] predicted that the eutectic growth at a constant growth rate occurs within a range of spacing values, near the extremum spacing, λ_{est}, which corresponds to the minimum undercooling. And they obtained the following expression for the average undercooling of the solid/liquid interface (SLI):

$$\Delta T = K_1 \lambda V + K_2 / \lambda \quad (3)$$

where, ΔT is the undercooling of the solidification front, λ is the inter-rod spacing, and K_1 and K_2 are summarized material parameters. A change in inter-rod spacing affects fibrous diameter accordingly. The fiber diameter (α) is related to the fiber spacing (λ) and the volume fraction of the fibers (V_f) by

$$\alpha^2 = gV_f\lambda^2 \quad (4)$$

where, g is the geometrical factor dependent on the fiber arrangement. In NiAl-Mo eutectic alloy, the fibers are arranged in a hexagonal pattern, and the parameter g can be proven to be $\sqrt{3/2}$ [16].

In our experiments, the volume fraction of the fibers, V_f varies from 14.65% to 15.02% when the growth rate varies from 2 μm/s to 40 μm/s. V_f changed in a narrow range, which is consistent with the results of Zhang's research[21]. Thus, assuming that V_f is constant at different solidification velocities, a change in inter-rod spacing affects fibrous diameter accordingly. Therefore Eq. (3) can be rewritten as:

$$\Delta T = K_1 \frac{1}{\sqrt{gV_f}} \alpha V + K_2 \sqrt{gV_f} \frac{1}{\alpha} \quad (5)$$

Eq. (5) predicts a wide range of fiber size for steady-state growth at certain growth rates. Fig.4a shows a significant variation in fibrous diameter at different growth velocities. The results indicate that the fiber size is not unique, but displays a limited range. The range decreases and becomes narrow when the growth rates increase. This is in accordance with the general eutectic growth theory developed by Jackson and Hunt (J-H theory). Although many efforts have been made of the spacing selection mechanism, the principle that influences the selection of spacing over this narrow band has not been built. In order to investigate the influence of the initial growth rate on the fiber size distributions, we also measured the distribution of fiber size in velocity sudden change experiments as shown in Fig.4b. Note that the distribution curves are nearly identical to that for the constant growth rate of 20 μm/s. It can be observed that fibrous diameter changes a little when the growth rate suddenly changes compared with the alloy at a constant growth rate of 20 μm/s. The average fiber size is about 550±20 nm, which was found to be the same at a given velocity for the two different initial conditions. Trivedi et al[22] discovered the same result that the final spacing was irrespective of the initial starting condition of eutectic spacing selection in lead-based alloy systems when the solidification velocity abruptly changed.

Meanwhile, according to the minimum undercooling criterion, Eq. (5) is referred to:

$$\alpha_{est}^2 V = \frac{K_2 g V_f}{K_1} \quad (6)$$

Fig.5 displays the variation in the average, minimum and maximum fiber size at different growth rates for NiAl-Mo system. It can be concluded that the smallest fiber size observed in the distribution curves of fibrous diameter in NiAi-Mo eutectic is close to the extremum fiber size obtained by Eq. (6). As discussed by Seetharaman and Trivedi[22], the observed smallest eutectic spacing appears to correspond to the value α_{est}, which gives minimum interface undercooling, showing that the eutectic spacing smaller than extremum value are unstable. And, the values of the average and

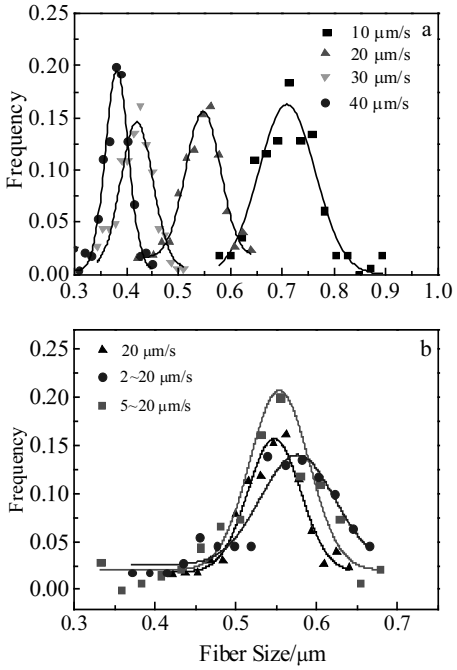

Fig.4 Distribution curves of fiber size in NiAl-Mo eutectic alloy for different growth velocities: (a) constant growth rates and (b) suddenly increased growth rate

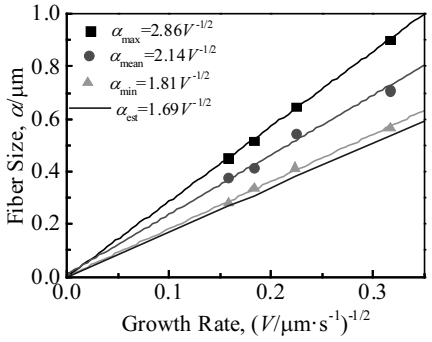

Fig.5 Variation in the average, maximum and minimum fiber size with different growth rates in the NiAl-Mo system

maximum fiber size are significantly larger than the theoretical value at the extremum condition in NiAl-Mo eutectic alloy.

2.2 Corrosion behaviour of NiAl-Mo eutectic alloy at different growth rates in 0.1 mol/L HCl

Fig.6a shows the potentiodynamic polarisation curves of NiAl-Mo eutectic alloy at various growth rates in 0.1 mol/L HCl aqueous solution. The corrosion current density (i_{corr}) was estimated from Tafel plots using both the cathodic and anodic branches of the polarization curves. From Fig.6a, it can be seen that the polarisation curve of the NiAl-Mo alloy at growth rate of 20 μm/s shifts to the upper left, which results in

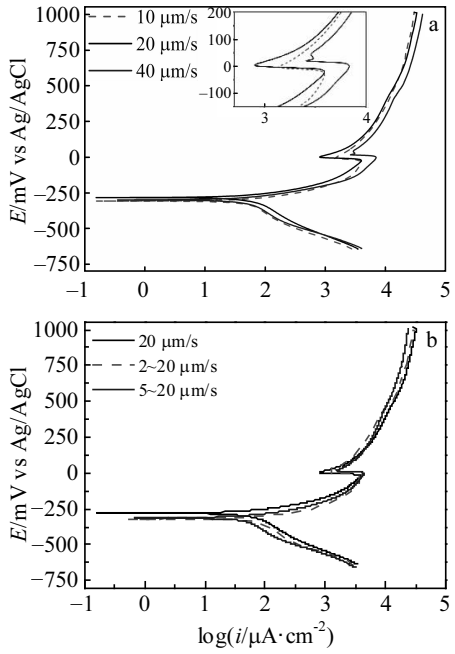

Fig.6 Potentiodynamic polarisation curves of NiAl-Mo eutectic alloy at different growth rates: (a) constant growth rates and (b) suddenly increased growth rate

a smaller corrosion current density (about 20.3 μA/cm^2) throughout each anodic polarisation range. And, E_{corr}, the corrosion potential (about –280 mV) at the growth rate of 20 μm/s is clearly higher than other growth rates. It is generally accepted that i_{corr} is indicative of metal corrosion kinetics, whereas E_{corr} reflects the thermodynamic characteristics of the system. It is further demonstrated from Fig.6a that a trend for the short passivity region in 0.1 mol/L HCl near the open circuit potential is noticeable at different growth rates. Also the passive region width is the broadest (about 50 mV) at growth rate of 20 μm/s. The passive region is due to the formation of the molybdenum oxide film in accordance with the Pourbaix diagrams for the Ni-Al-Mo system. The increase of the current readings around 50 mV represents the breakdown potential of the molybdenum oxide film. The optimal potential for NiAl matrix dissolution and wire passivation was found to be 50 mV (of about 250 mV SHE). Additionally, the curve for the alloy at growth rate of 40 μm/s exhibit a spike which seems to be caused by pitting initiation and repassivation, as similarly reported in the studies carried out by Osório[11]. Therefore, the alloy at growth rate of 20 μm/s has a greater proneness to resist corrosion than those at 10 and 40 μm/s.

The corrosion resistance of directionally solidified NiAl-Mo eutectic alloy at different growth rates is affected due to the following two possibilities: eutectic spacing and morphologies. The both spacing and diameter decrease with the growth rate increasing in a directionally solidified

NiAl-Mo alloy. Corrosion resistance could be improved through reducing phase spacing and diameter. However, a comparison of potentiodynamic polarisation curves for NiAl-Mo alloy at growth rates of 20 and 40 μm/s suggests that the former has greater corrosion resistance. Hence, the factor which influences the corrosion behaviour of the NiAl-Mo eutectic alloy is not only eutectic spacing.

In order to further clarify the influence of the morphologies on the corrosion resistance, the positions along the directionally solidified NiAl-Mo alloys with different values of V/V_1 were for corrosion tests, which are indicated in Fig.2 (P_1 and P_2).

In the position P_2, the typical hypoeutectic NiAl-Mo alloy microstructure consists of an intermetallic phase (NiAl dendritic) and a eutectic mixture in the interdendritic region formed by Mo-phase and intermetallic NiAl particles, whereas, a eutectic mixture was only observed in the position P_1. In addition, the average fiber size is about 550 nm for three samples. Fig.6b shows the potentiodynamic polarisation curves of NiAl-Mo eutectic alloy with different eutectic morphologies. It can be clearly seen that the alloy at constant growth rate of 20 μm/s has a better corrosion behavior. However, the optimal potential of Mo nanowires spanning for different eutectic morphologies are the same, which is always about 250 mV SHE for NiAl phase dissolution and Mo nanowires spanning.

Fig.7 shows selected microstructures of NiAl-Mo alloys at different growth rates after electrochemical tests in a 0.1 mol/L HCl solution. Fig.7b indicates the NiAl-Mo alloy exhibits a cellular microstructure at the growth rate of 40 μm/s, and it was observed that fibers do not grow parallel to each other within the cells but diverge toward colony boundaries and tend to increase in thickness as they approach it. In the NiAl-Mo eutectic alloy of 40 μm/s solidification velocity, it can be seen that most of holes are distributed along the cell boundaries, which reveals the corrosion of NiAl-Mo alloy may firstly occur in the boundary. Fig.7c clearly shows a large number of nanowires which are standing upright to the surface and parallel, but the fibers diverge toward colony boundaries as shown in Fig.7d. The wire has a length of 70 μm and fibrous diameter of 300 nm. An aspect ratio is calculated to be more than 230.

In the process of potentiodynamic polarization, the main transition is about the NiAl phase dissolution while passivating the fibrous minor phase results in Mo nanowires spanning along the central part of the sample. Considering the anodic reaction, the basic reaction consists of the reaction $Al \rightarrow Al^{3+}+3e^-$ and $Ni \rightarrow Ni^{2+}+2e^-$, as well as cathodic reaction $2H^++2e^- \rightarrow H_2$. The combined Pourbaix diagram also displays that molybdenum should exist as MoO_3 under these conditions, preventing the dissolution of molybdenum. A higher potential would favor the MoO_3 formation resulting in a larger oxide thickness.

From Fig.8, it is clear that corrosion pits present grain boundary and cellular boundary for the alloys at growth rate of 20 and 5~20 μm/s, respectively. Some of them even contact with each other and form deep ravines. Most of holes are distributed along the boundaries, but some corrosion damage is still found in the grains and cells. This shows that the dominant corrosion mechanism is grain-boundary corrosion. Grain and cellular boundaries are regions with higher level of energy due to distortions and deformations caused by growth

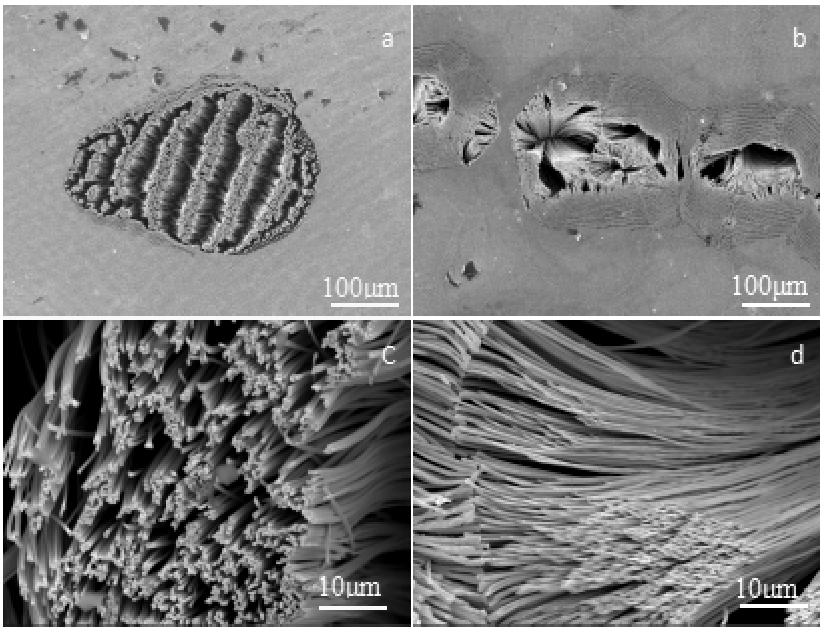

Fig.7 SEM images of NiAl-Mo sample after potentiodynamic polarisation in 0.1 mol/L HCl: (a, c) 20 μm/s and (b, d) 40 μm/s

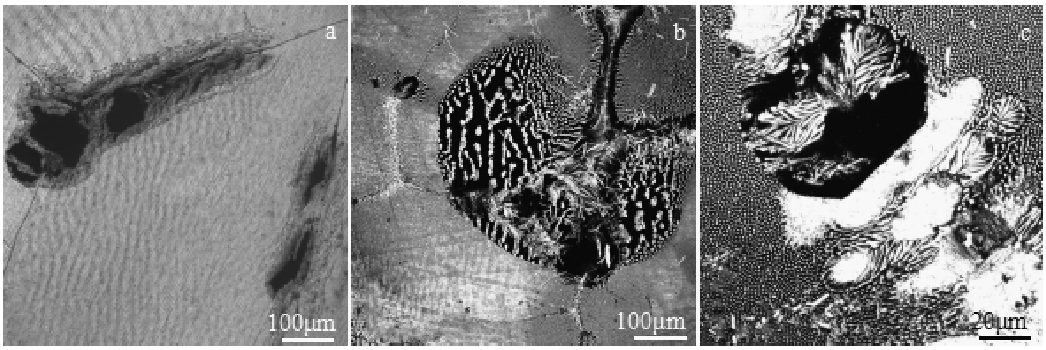

Fig.8 Corrosion morphologies of NiAl-Mo sample after potentiodynamic polarisation in 0.1 mol/L HCl: (a) 20 μm/s, (b) 5~20 μm/s, and (c) 2~20 μm/s

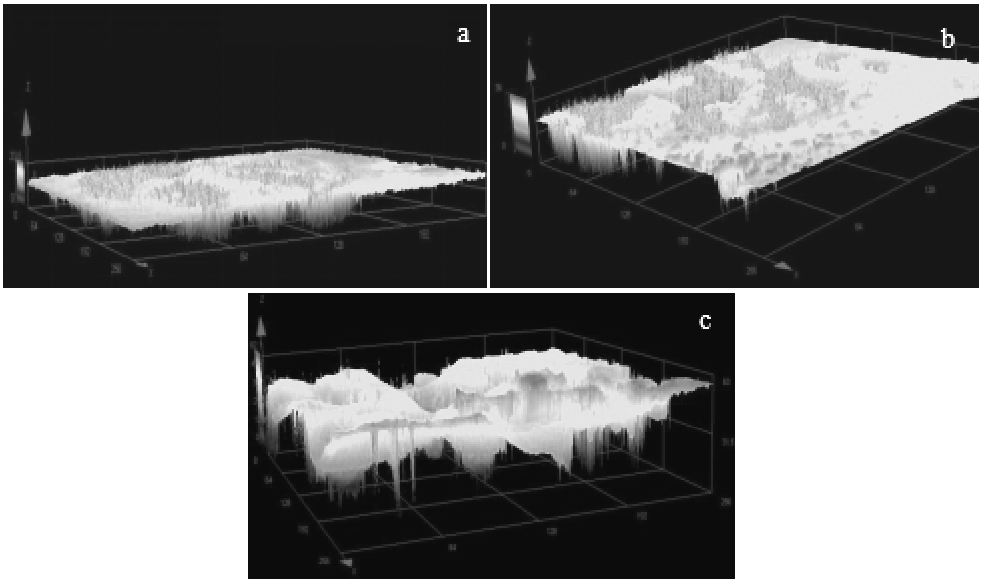

Fig.9 Three-dimension morphologies of NiAl-Mo alloy with different growth rates after potentiodynamic polarisation in 0.1 mol/L HCl solution: (a) 20 μm/s, (b) 5~20 μm/s, and (c) 2~20 μm/s

during solidification being more susceptible to the corrosion action. The alloy at growth rate of 20 μm/s exhibits fewer boundaries, providing a better galvanic protection compared to the alloy at 5~20 μm/s, which will be subjected to a more extensive corrosion action. From Fig.8c, it can be seen that interdendritic corrosion takes place, which are caused by the composition segregation between branches and interdendrites. And NiAl phase consists of higher content of Al compared to eutectic mixture. The corrosion initiates mostly in the enrichment zone of Al atoms. Hence, corrosion is more easily to occur for NiAl dendrite. The sample with dendritic structure exhibits more susceptible grain boundaries, and there are more interdendritic imperfection and more regions for corrosion to occur.

Fig.9 shows the three-dimensional morphologies of NiAl-Mo alloys after potentiodynamic polarisation in 0.1 mol/L HCl. It can be observed that the depth of the alloy at a constant growth rate of 20 μm/s is shallower than those of samples at suddenly changed growth rates. In addition, the alloy of 2~20 μm/s growth rate is the most bumpy of the three alloys. In general, the electrochemical behaviour concerning tests in a 0.1 mol/L HCl solution is mainly affected by the size and microstructure. Note that the fiber size for NiAl-Mo alloys at 2~20 and 5~20 μm/s are similar to that of the alloy at a constant growth rate of 20 μm/s. It is found that the corrosion resistance of the directionally solidified samples rises in the order of dendritic structure<cellular structure< planar structure. The results are in agreement with the electrochemical tests.

3 Conclusions

1) Extensive fiber size measurements in directionally

solidified NiAl-Mo eutectic alloys show that the fibrous size is not a unique value but display a limited narrow range, which decreases with the increase of the growth rate. According to the comparison between the experimental data and the theoretical model, it can be concluded the smallest fiber size observed in their distribution is close to the extremum fiber size.

2) The potentiodynamic polarization curves exhibit active-passive corrosion in 0.1 mol/L HCl, which shows the NiAl-Mo eutectic at growth rate of 20 μm/s has the better corrosion resistance. Eutectic spacing and interface morphology influence the corrosion resistance of directionally solidified NiAl-Mo eutectic. The optimal potential for NiAl phase dissolution and Mo fiber passivation is about 250 mV SHE.

3) The dynamical experiment, where the initial growth rate suddenly changes, shows that the microstructure of directionally solidified NiAl-Mo alloy transforms from planar to cellular and dendritic structures as the value of V/V_1 increases. It has been evidenced that the sample with the planar solid-liquid interface possesses better general corrosion resistance compared with the results of cellular and dendritic structure samples, which is due to the smallest susceptible grain boundaries.

References

1 Chen J Y, Wiley B J, Xia Y N. *Langmuir*[J], 2007, 23(8): 4120
2 Jin R C, Cao Y W, Mirkin C A *et al*. *Science*[J], 2001, 294(5548): 1901
3 Cui S W, Yin X Y, Yu Q L *et al*. *Corrosion Science*[J], 2015, 98: 471
4 Yasakau K A, Tedim J, Zheludkevich M L *et al*. *Corrosion Science*[J], 2012, 58: 41
5 Wirtz M, Martin C R. *Advanced Materials*[J], 2003, 15(5): 455
6 Kamat P V, Huehn R, Nicolaescu R. *Journal of Physical Chemistry B*[J], 2002, 106(4): 788
7 Hassel A W, Smith A J, Milenkovic S. *Electrochimica Acta*[J], 2006, 52(4): 1799
8 Su H P, Shen J, Zhang J F *et al*. *Rare Metal Materials and Engineering*[J], 2010, 39(6): 1009 (in Chinese)
9 Ren H G, Wang W J, Gao J J *et al*. *Rare Metal Materials and Engineering*[J], 2016, 45(1): 222 (in Chinese)
10 Milenkovic S, Hassel A W, Schneider A. *Nano Letters*[J], 2006, 6(4): 794
11 Osório W R, Peixoto L C, Canté M V *et al*. *Electrochimica Acta*[J], 2010, 55(13): 4078
12 Peixoto L C, Osório W R, Garcia A. *Journal of Power Sources*[J], 2009, 192(2): 724
13 Gali A, Bei H, George E P. *Acta Materialia*[J], 2010, 58(2): 421
14 Yang L Y, Li S M, Chang X Q *et al*. *Acta Materialia*[J], 2015, 97: 269
15 Chou Y L, Yeh J W, Shih H C. *Corrosion Science*[J], 2010, 52(8): 2571
16 Bei H, George E P. *Acta Materialia*[J], 2005, 53(1): 69
17 Dudová M, Kuchařová K, Barták T *et al*. *Scripta Materialia*[J], 2011, 65(8): 699
18 Smith V G, Tiller W A, Rutter J W. *Canadian Journal of Physics*[J], 1955, 33(12): 723
19 Cline H E, Anthony T R. *Acta Metallurgica*[J], 1971, 19(6): 491
20 Jackson K A, Hunt J D, Jackson K H. *AIME Met Soc Trans*[J], 1966, 236: 1129
21 Zhang J F, Shen J, Shang Z *et al*. *Intermetallics*[J], 2012, 21(1): 18
22 Trivedi R, Mason J T, Verhoeven J D *et al*. *Metallurgical Transactions A*[J], 1991, 22(10): 2523

纤维尺寸和界面形态对定向凝固 NiAl-9Mo 共晶合金电化学腐蚀性能的影响

郭俊波，钟　宏，刘振鹏，杨鲁岩，李双明

(西北工业大学 凝固技术国家重点实验室，陕西 西安 710072)

摘　要：由于凝固组织对腐蚀有着重要的影响，本文主要目地获取最优组织形态和电化学参数生产钼纳米丝。研究表明 NiAl-Mo 共晶合金定向凝固下，组织由基体 NiAl 相和纤维 Mo 相共生耦合生长。随着抽拉速率从 10 μm/s 增大到 40 μm/s 时，纤维尺寸从 800 nm 减小到 300 nm，界面形态也从平界面变化成胞界面。同时在 0.1 mol/L HCl 电解液下测量其极化曲线，发现凝固速率为 20 μm/s 时耐腐蚀性能最好。对于 NiAl-Mo 共晶合金，影响电化学腐蚀性能的不仅仅是纤维尺寸，还取决于界面形貌。为了更进一步研究界面形态对腐蚀的影响，设计了跃迁变速实验，实验表明定向凝固组织形貌会随着变速比的增大从平界面变成胞界面，最后变成枝界面，然而最后的纤维尺寸和变速比无关，和恒速抽拉相同。极化曲线表明平界面有着最好的耐腐蚀性能。

关键词：定向凝固；NiAl-Mo 共晶合金；界面形貌；耐腐蚀性能

作者简介：郭俊波，男，1992 年生，硕士生，西北工业大学凝固技术国家重点实验室，陕西 西安 710072，E-mail: guojunbo@mail.nwpu.edu.cn